Supporting Information for

Rational Engineering and Synthesis of Pyrene and Thiazolo[5,4-d]thiazole-Functionalized Conjugated Microporous Polymers for Efficient Supercapacitor Energy Storage

Abdul Basit[a], Yang-Chin Kao[a], Yasser A. El-Ossaily[b], Shiao-Wei Kuo[a,c]* and Mohamed Gamal Mohamed[a,d]*

[a]Department of Materials and Optoelectronic Science, Center for Functional Polymers and Supramolecular Materials, National Sun Yat-Sen University, Kaohsiung 804, Taiwan.

[b]Department of Chemistry, College of Science, Jouf University, P.O.Box 2014, Sakaka, Saudi Arabia.

[c]Department of Medicinal and Applied Chemistry, Kaohsiung Medical University, Kaohsiung 807, Taiwan.

[d]Department of Chemistry, Faculty of Science, Assiut University, Assiut 71516, Egypt.

Corresponding authors:

E-mail: kuosw@faculty.nsysu.edu.tw (S. W. Kuo) and mgamal.eldin34@gmail.com (M. G. Mohamed).

Characterization

FTIR spectra were collected on a Bruker Tensor 27 FTIR spectrophotometer with a resolution of 4 cm^{-1} by using the KBr disk method. ^{13}C nuclear magnetic resonance (NMR) spectra were examined by using an INOVA 500 instrument with DMSO-d_6 and $CDCl_3$ as the solvent and TMS as the external standard. Chemical shifts are reported in parts per million (ppm). Solid-state ^{13}C NMR was measured by JEOL JNM-LA300 spectrometer and standard CPMAS probe at 75.577 MHz. The thermal stabilities of the samples were performed by using a TG Q-50 thermogravimetric analyzer under a N_2 atmosphere; the sample (ca. 5 mg) was put in a Pt cell with a heating rate of 20 °C min^{-1} from 100 to 800 °C under a N_2 flow rate of 60 mL min^{-1}. Solid-state ^{13}C NMR was measured by JEOL JNM-LA300 spectrometer and standard CPMAS probe at 75.577 MHz. The morphologies of the polymer network samples were examined by Field emission scanning electron microscopy (FE-SEM; JEOL JSM7610F) and transmission electron microscope (TEM) using a JEOL-2100 instrument at an accelerating voltage of 200 kV. X-ray Photoelectron Spectroscopy (XPS): XPS was measured on a X-ray Photoelectron Spectrometer System (Thermo Scientific). The X-ray monochromator used micro-focused Al-Kα radiation. Surface area and porosity measurements of samples weighing approximately 40-60 mg were conducted using the BEL MasterTM/BEL simTM (version 3.0.0) apparatus. Nitrogen (N_2) adsorption and desorption isotherms were generated by gradually exposing the samples to ultrahigh-purity N_2 gas, reaching pressures of up to about 1 atmosphere, while maintaining a temperature of 77 K in a liquid nitrogen bath. Before these measurements, the samples underwent a degassing process at 150 °C for 8 h. The instrument's software was utilized to calculate surface parameters using the BET adsorption models. Furthermore, the pore size of the prepared samples was determined using nonlocal density functional theory (NLDFT).

Electrochemical Analysis

Working Electrode Cleaning: Before use, the glassy carbon electrode (GCE) was polished several times with 0.05-µm alumina powder, washed with EtOH after each polishing step, cleaned through sonication (5 min) in a water bath, washed with EtOH, and then dried in air.

Electrochemical Characterization: The electrochemical experiments were performed in a three-electrode cell using an Autolab potentiostat (PGSTAT204) and 1 M KOH as the aqueous electrolyte. The GCE was used as the working electrode (diameter: 5.61 mm; 0.2475 cm^2); a Pt wire was used as the counter electrode; Hg/HgO (RE-1B, BAS) was the reference electrode. All reported potentials refer to the Hg/HgO potential. A slurry was prepared by dispersing the Py-Ph-TzTz CMP or Py-Th-TzTz CMP (50%), carbon black (40%), and Nafion (10%) in a mixture of (EtOH/ H_2O) (200 µL: 800 µL) and then sonicated for 2 h. A portion of this slurry (10 µL) was pipetted onto the tip of the electrode, which was then dried in air for 30 min before use. The electrochemical performance was studied through CV at various sweep rates (5–200 mV s^{-1}) and through the GCD method in the potential range of +0 to -1 V at varying current densities (0.5-20 A/g) and CV at different sweep rates (5-200 mV/sec). The equation below was used to compute the specific capacitance based on the CV curves:

$$Q = \frac{\int IdV}{2\ m\ v}$$

The specific capacitance was calculated from the GCD data using the equation:

$$C_s = (I\Delta t)/(m\Delta V)$$

Where C_s (F g^{-1}) is the specific capacitance of the supercapacitor, I (A) is the discharge current, ΔV (V) is the potential window, Δt (s) is the discharge time, and m (g) is the mass of the NPC on the electrode.

Electrochemical Analysis in Two-Electrode Symmetric Supercapacitor System

The slurry prepared by mixing Py-Ph-TzTz CMP or Py-Th-TzTz CMP, carbon black, and Nafion (10 wt. %) was coated onto a flexible Kuraray carbon paper (0.1 mm in thickness) with an effective area of 1 cm × 1 cm and then dried at 100 °C overnight in a vacuum oven. The mass loading of active material on the current collector was 0.8 mg cm^{-2}. The two working electrodes were separated with filter paper and infiltrated with potassium hydroxide (1 M) aqueous solution.

The specific capacitance was calculated from galvanostatic charge-discharge experiments using the following equation:

$$Cs = 2 \times (I\Delta t)/(m\Delta V)$$

Where Cs (F/g) is the specific capacitance of the supercapacitor, I (A) is the discharge current, ΔV (V) is the potential window, Δt (s) is the discharge time, and m (g) is the mass of porous carbon on the one electrode. The energy density (E, Wh kg^{-1}) and power density (P, W kg^{-1}) were calculated using the equations.

$$E = C(\Delta V)^2/(4 \times 7.2)$$

$$P = E/(t/3600)$$

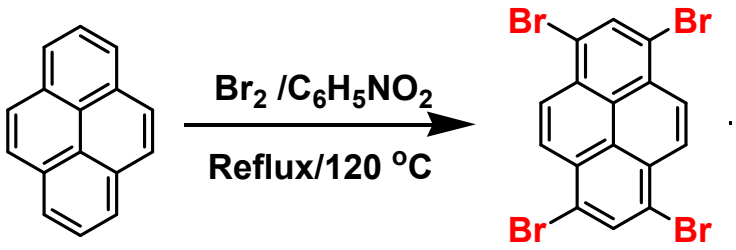

Scheme S1. Synthesis of Py-Br_4.

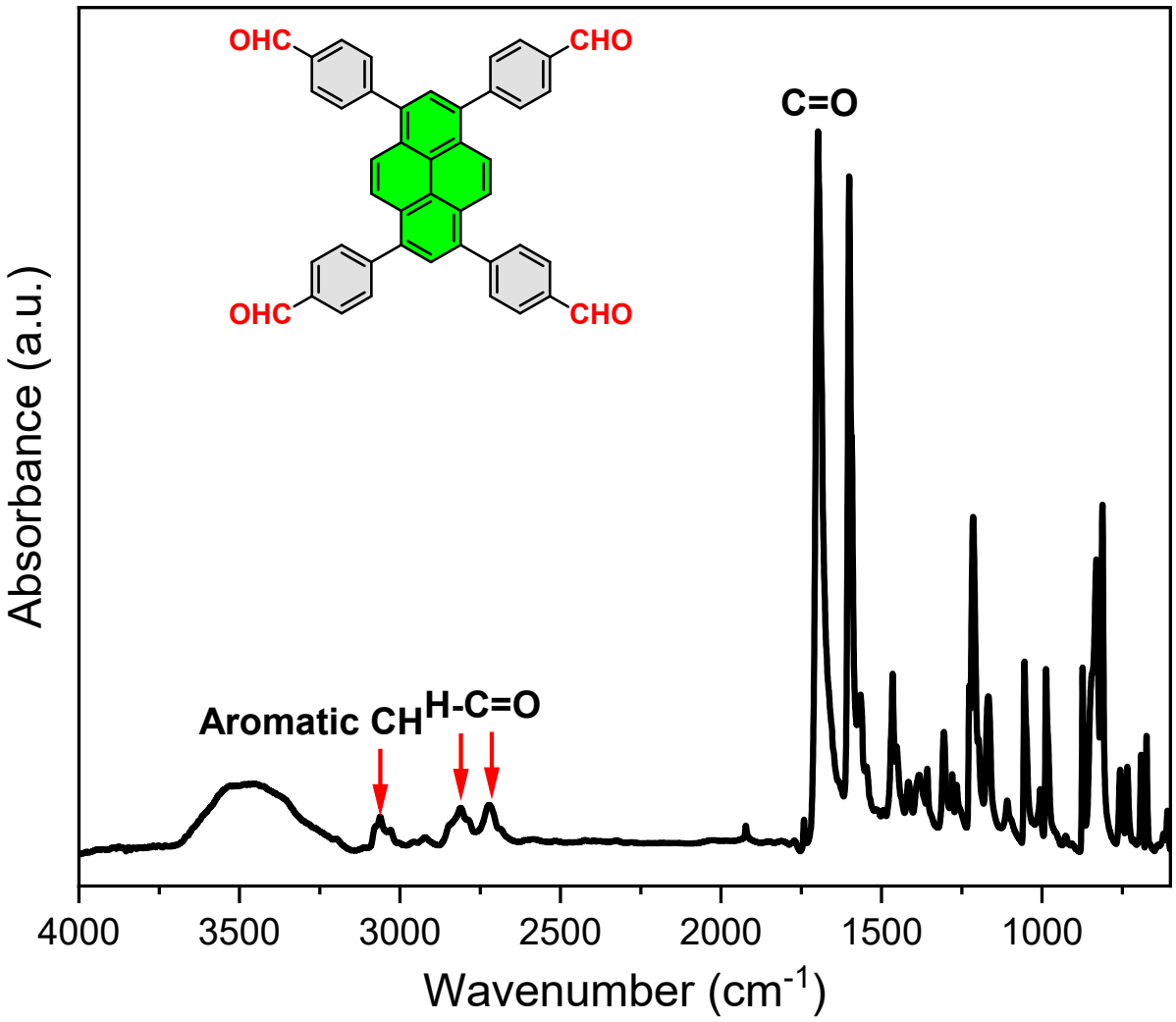

Figure S1. FTIR spectrum of Py-Ph-4CHO.

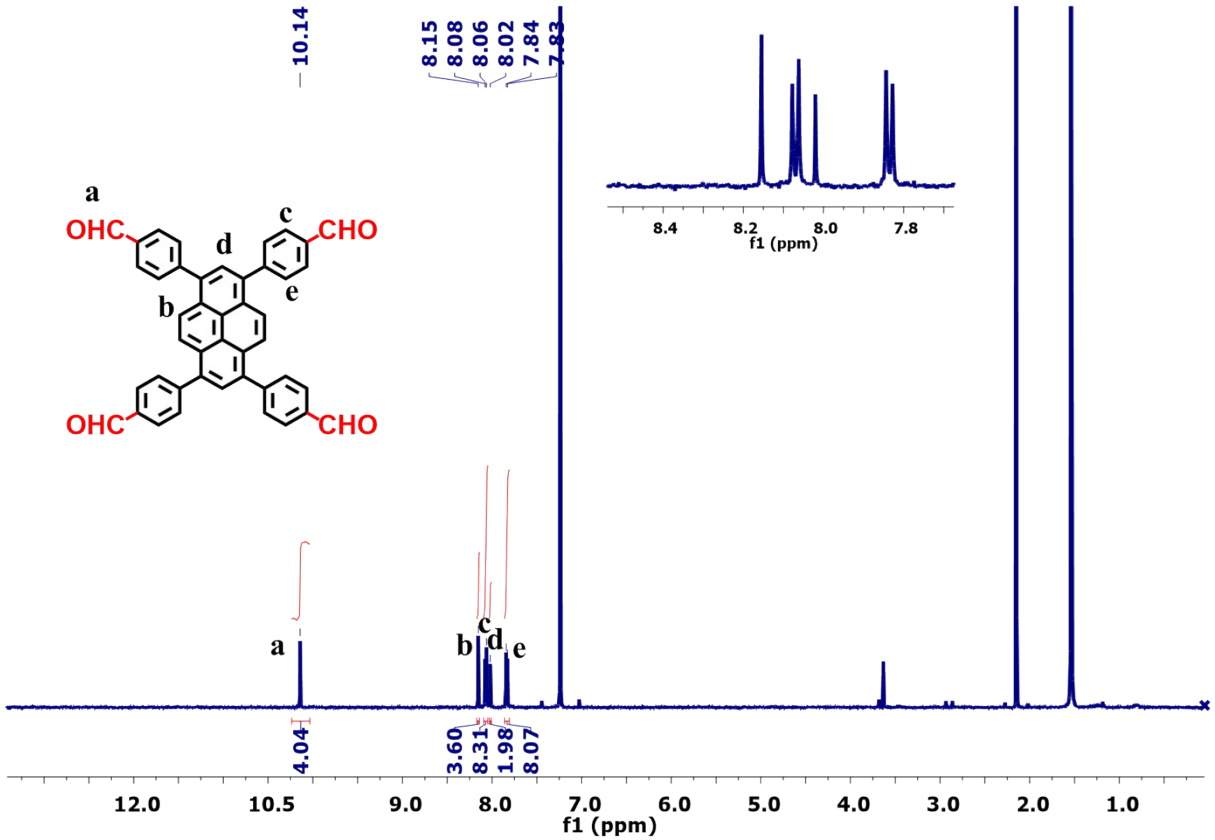

Figure S2. ^{1}H-NMR spectrum of Py-Ph-4CHO.

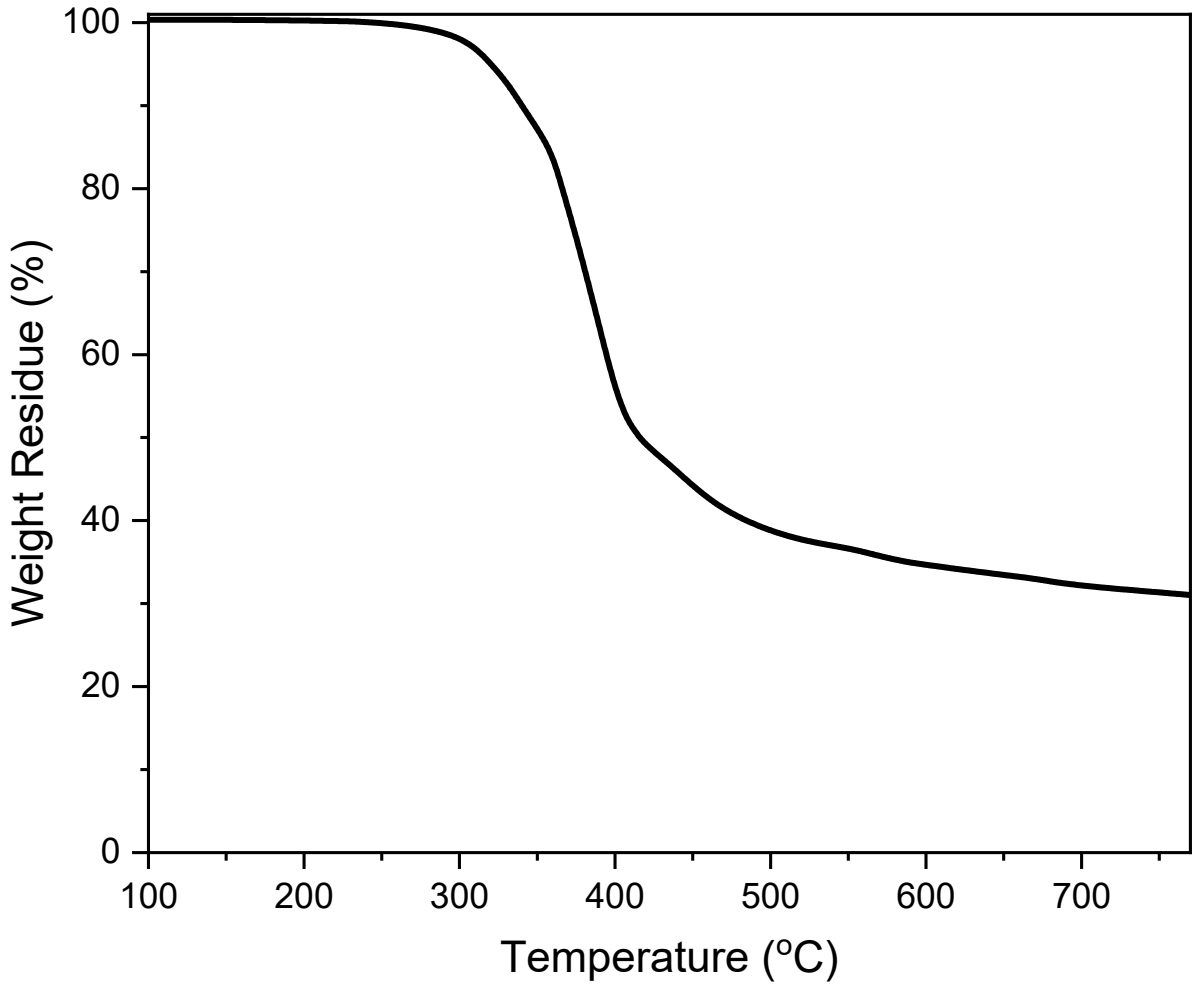

Figure S3. TGA spectrum of Py-Ph-4CHO.

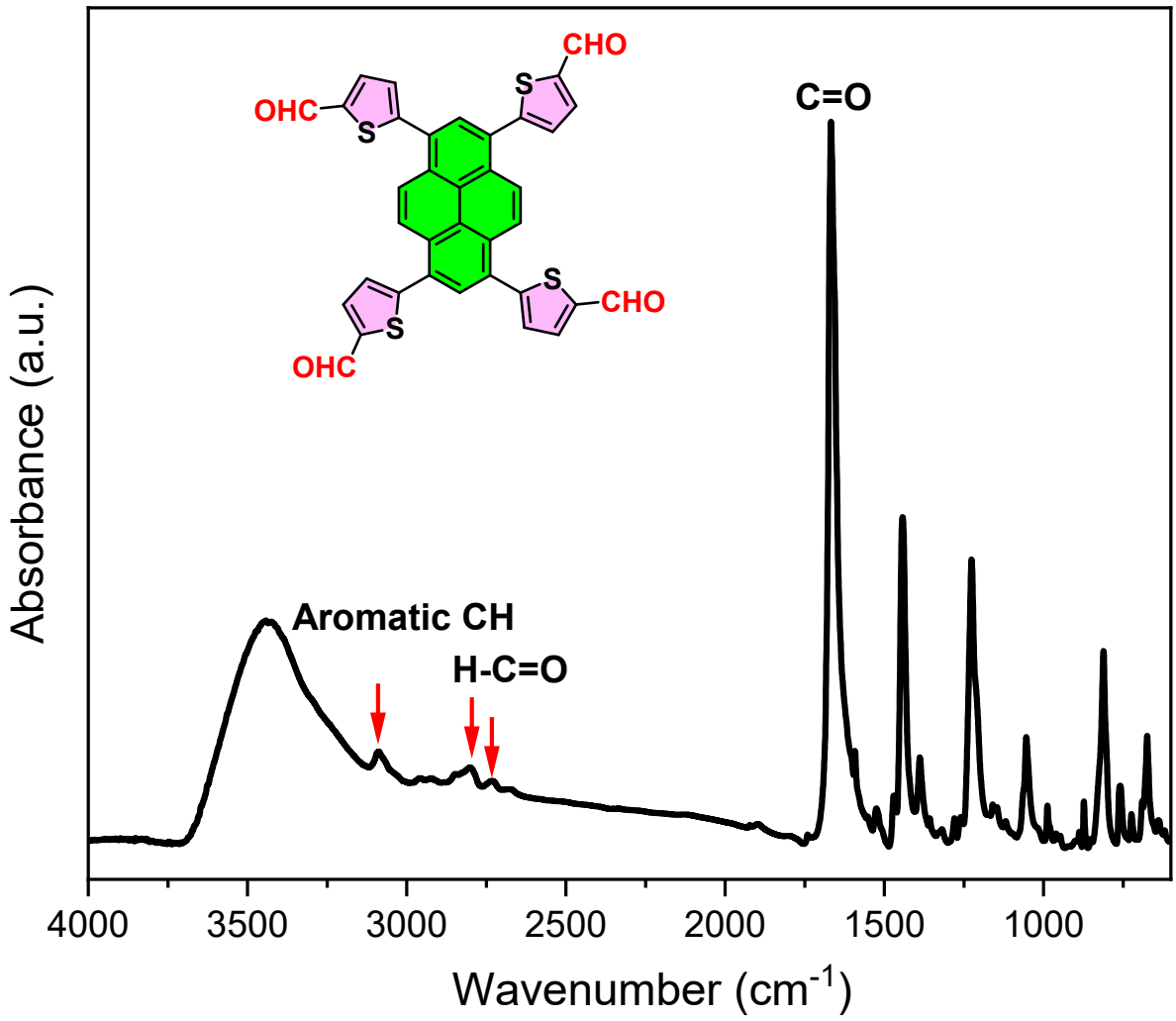

Figure S4. FTIR spectrum of Py-Th-4CHO.

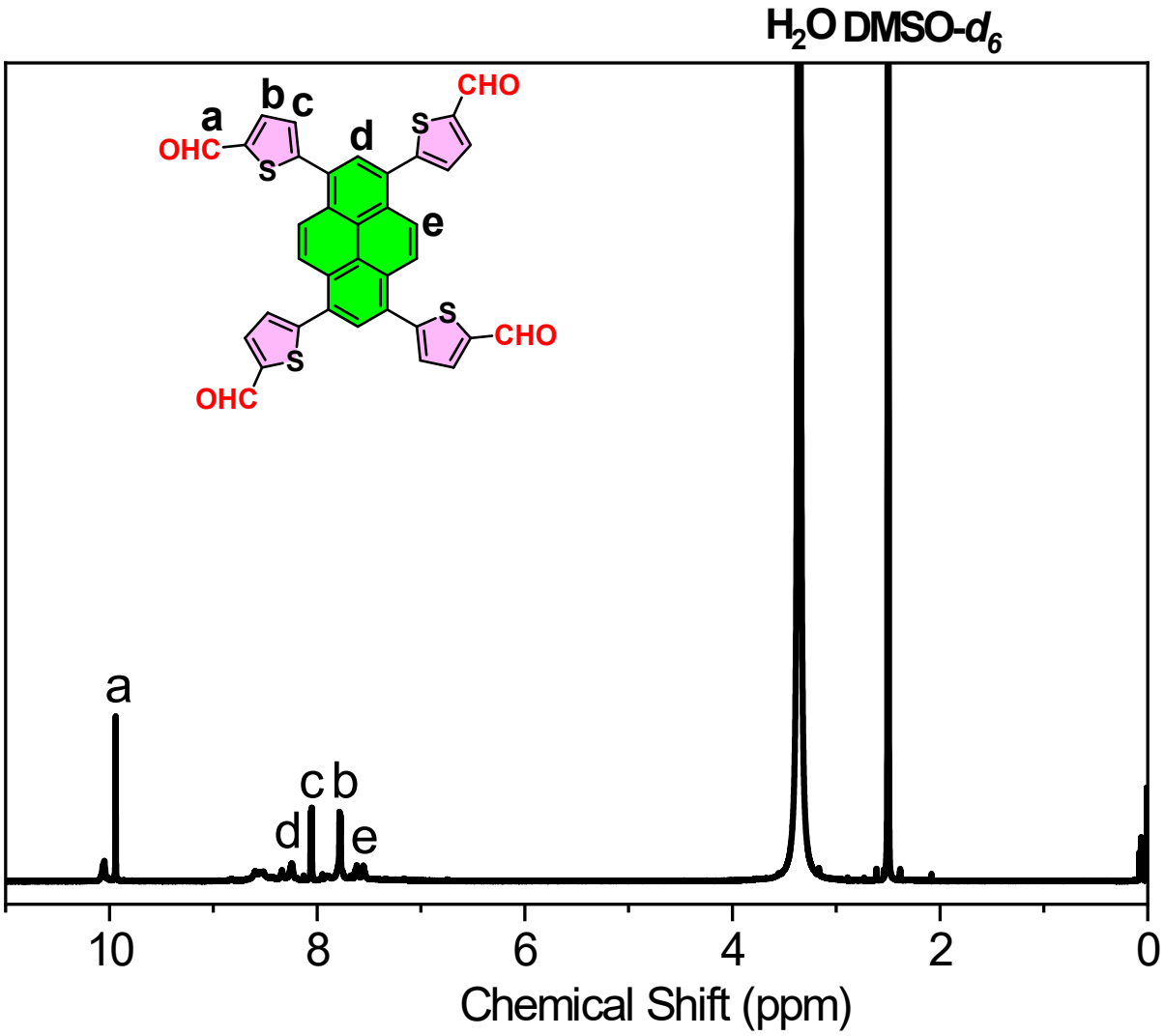

Figure S5. [1]H-NMR spectrum of Py-Th-4CHO.

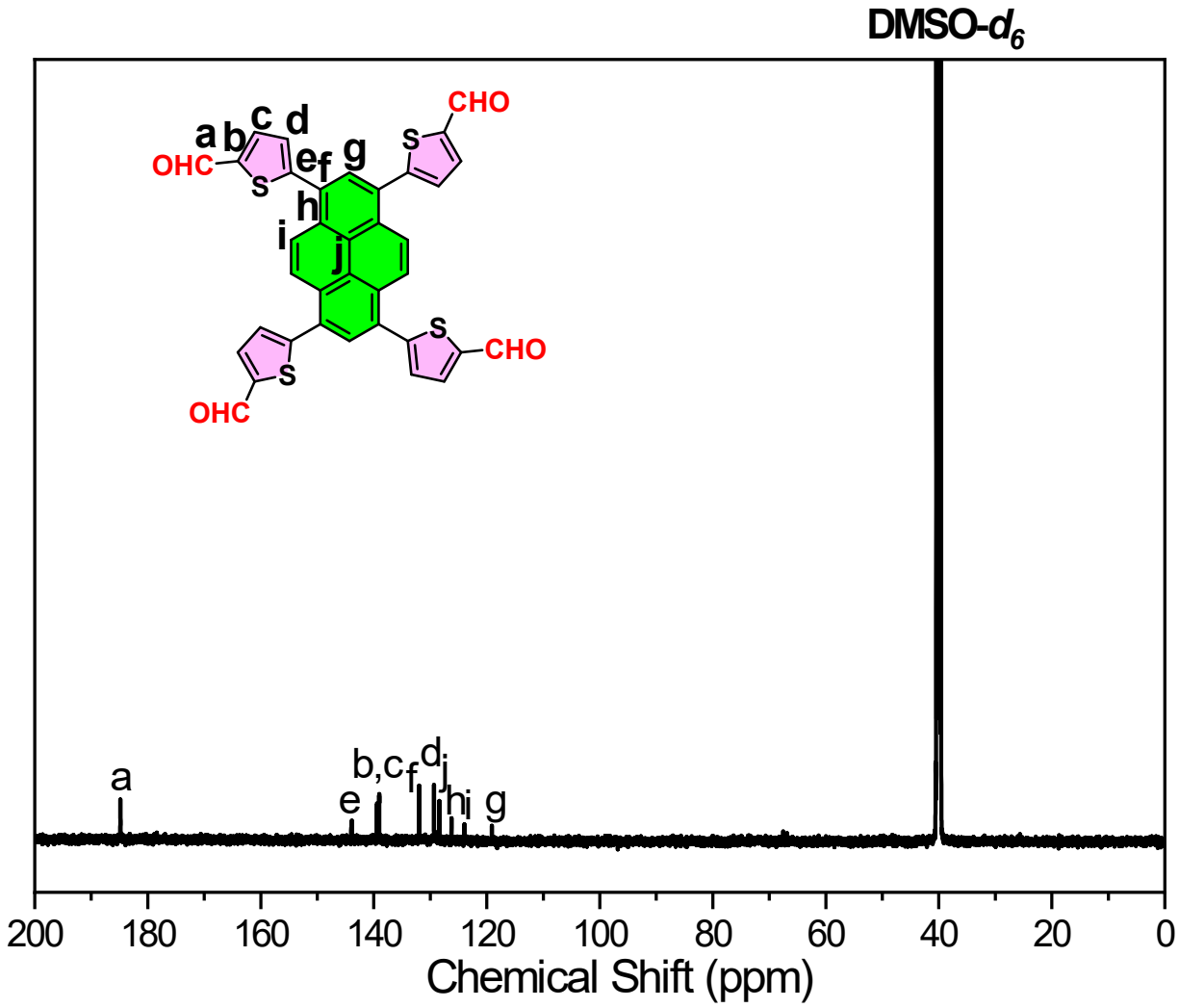

Figure S6. ^{13}C-NMR spectrum of Py-Th-4CHO.

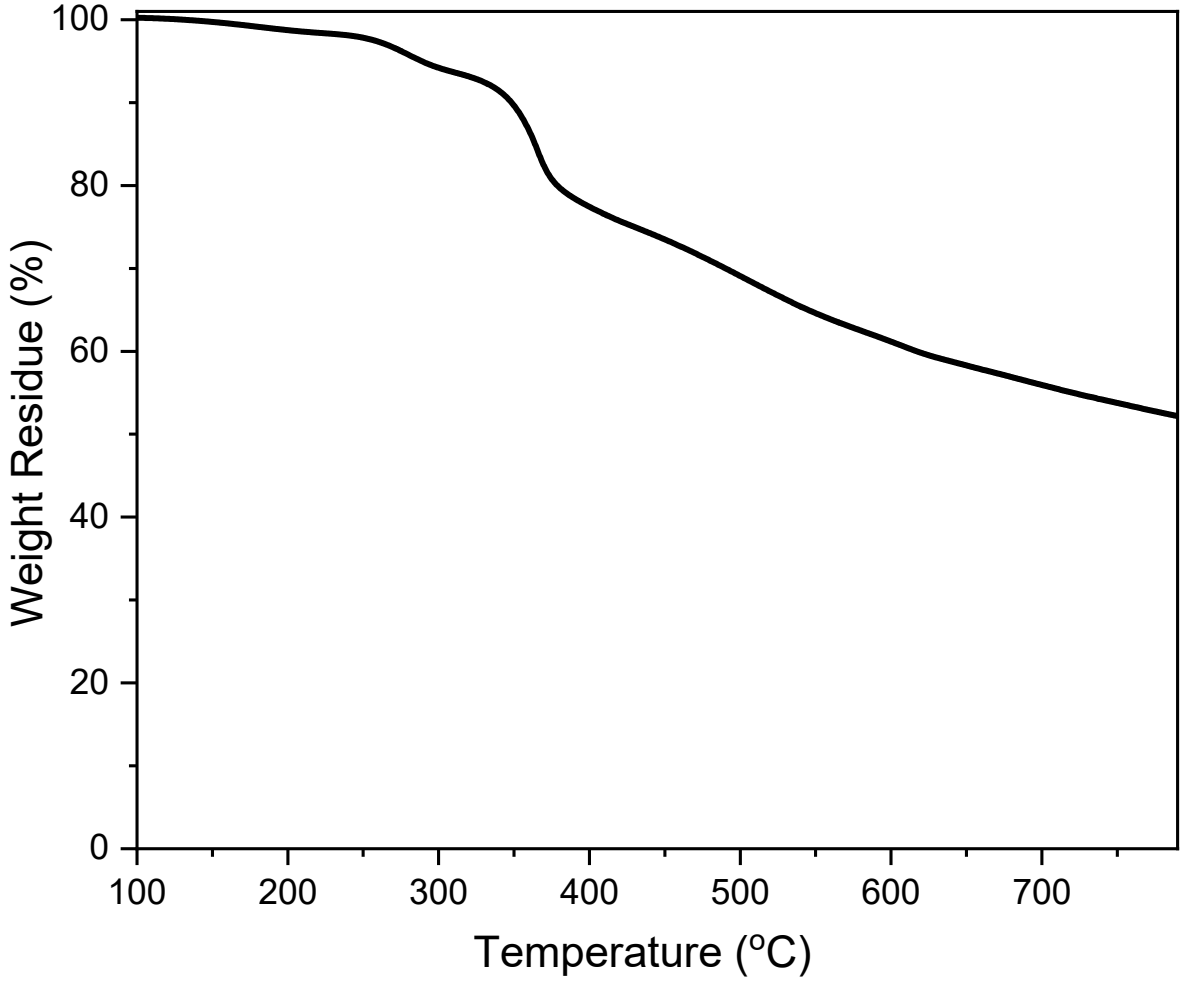

Figure S7. TGA traces of Py-Th-4CHO.

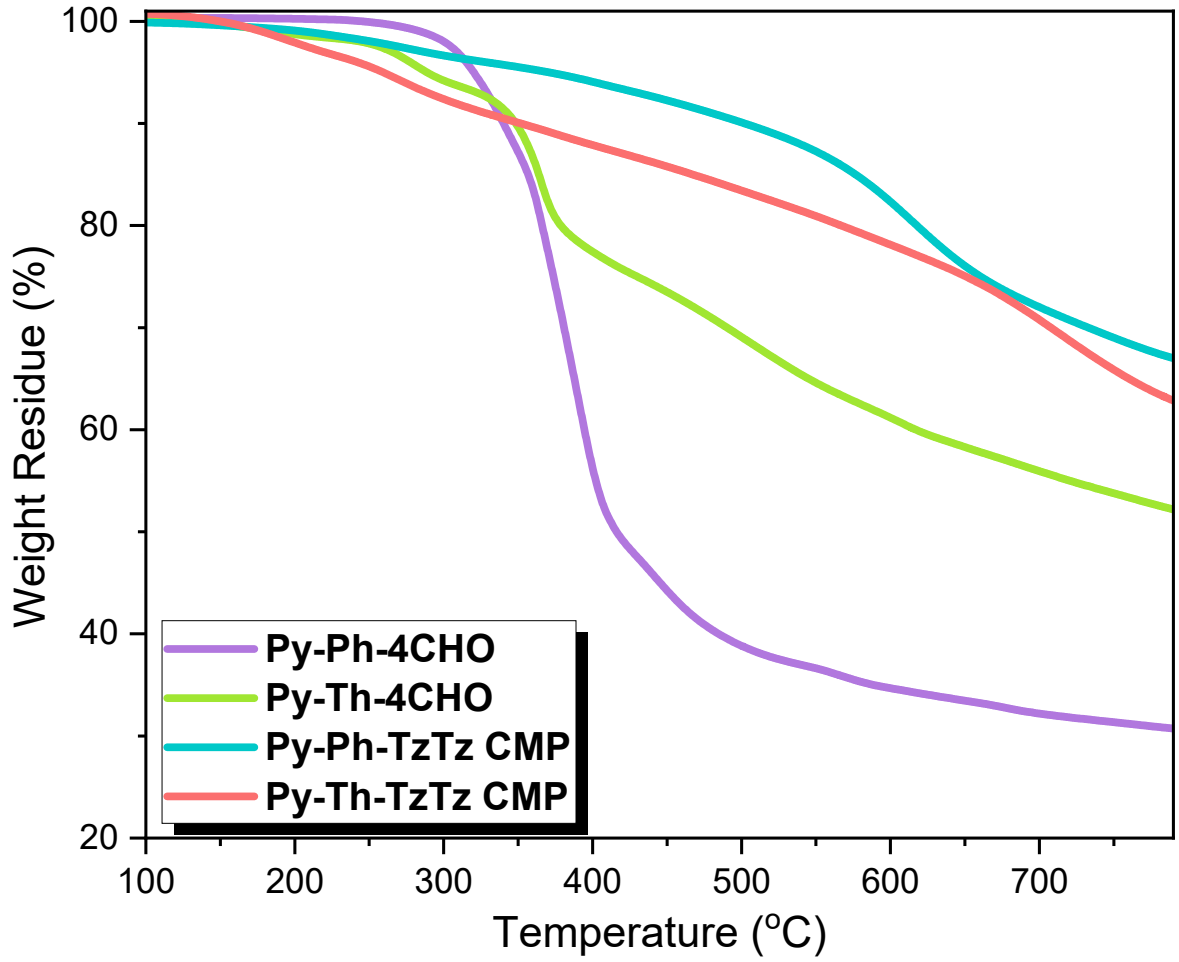

Figure S8. TGA traces of Py-Ph-4CHO, Py-Th-4CHO, Py-Ph-TzTz CMP, and Py-Th-TzTz CMP.

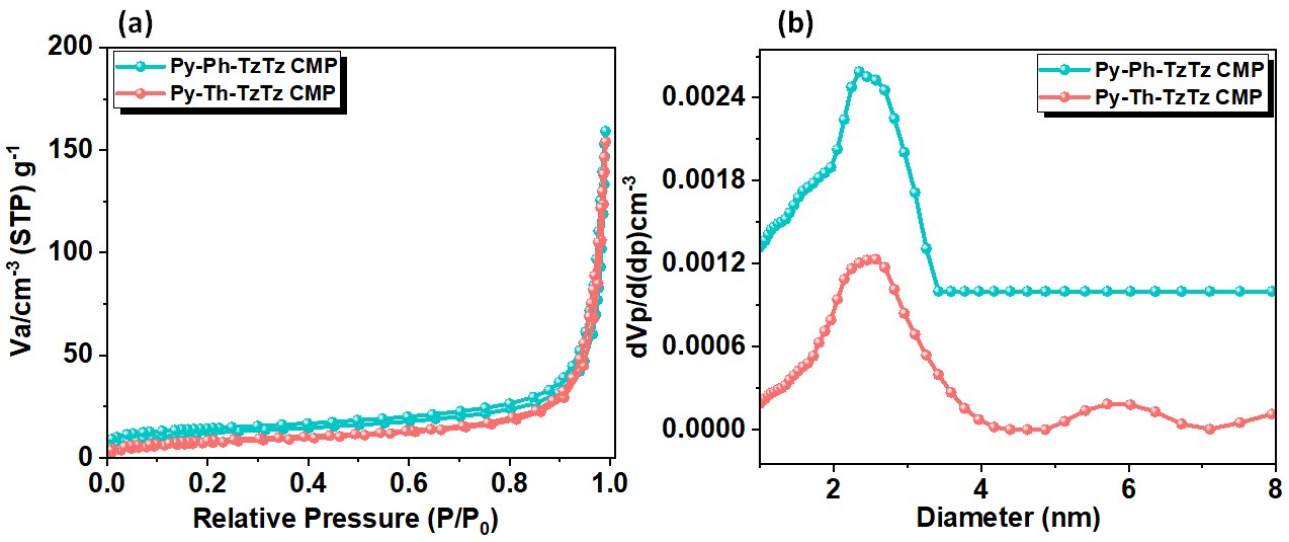

Figure S9. (a) N_2 adsorption-desorption isotherm and (b) pore size distribution curves of Py-Ph-TzTz CMP and Py-Th-TzTz CMP.

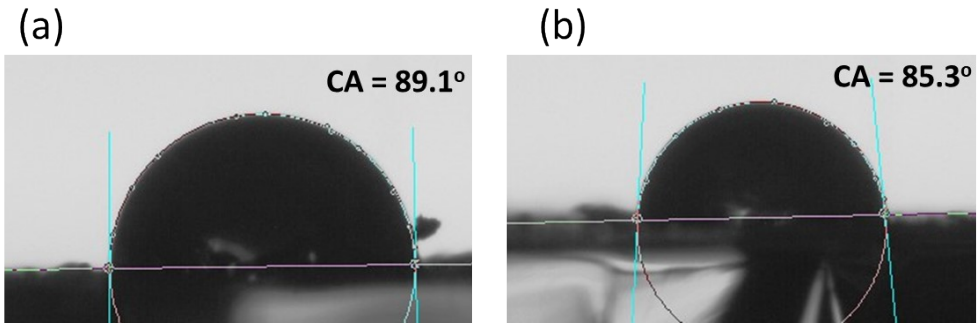

Figure S10. Water Contact angle (WCA) measurements for (a) Py-Ph-TzTz CMP and (b) Py-Th-TzTz CMP.

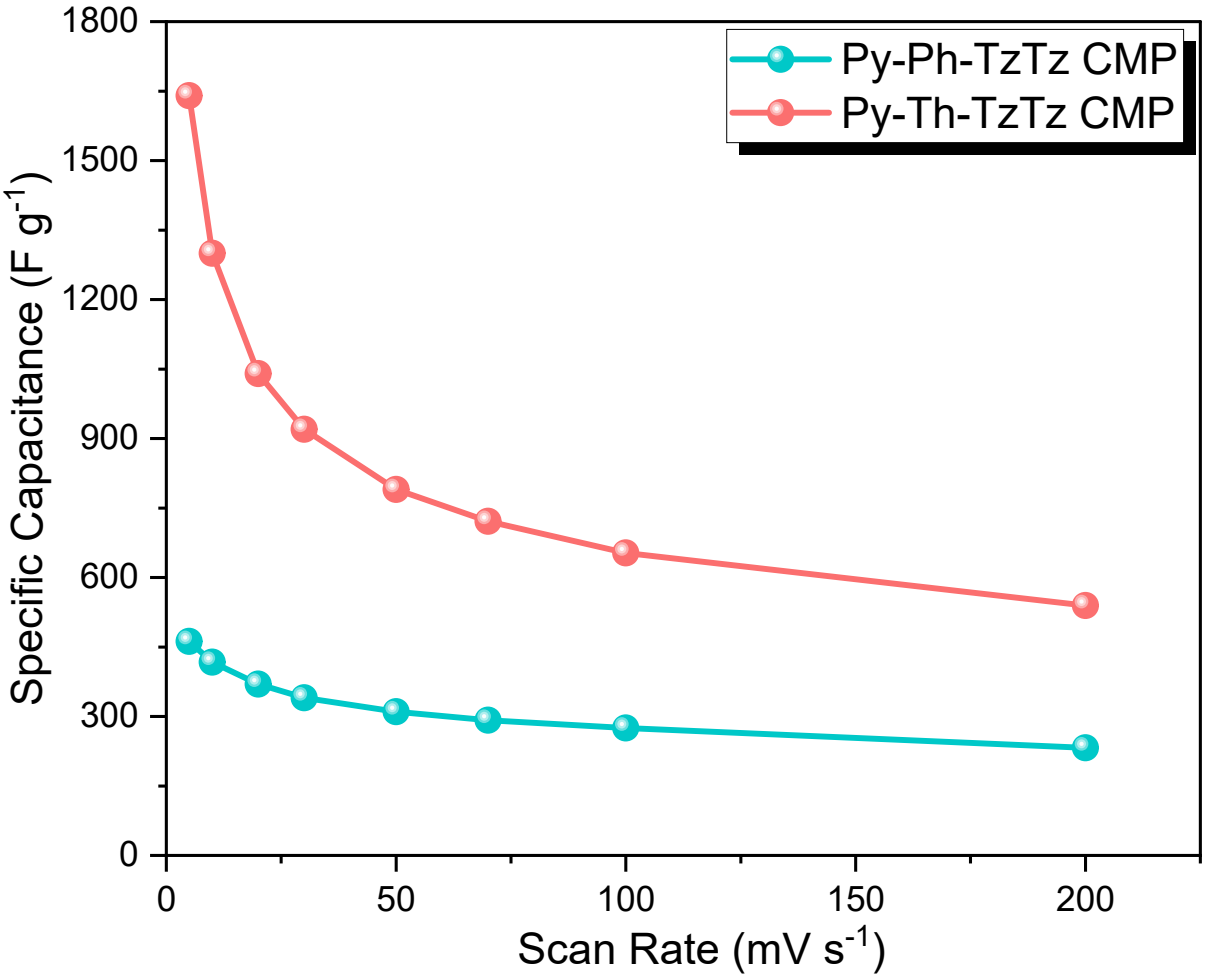

Figure S11. Specific capacitance values of Py-Ph-TzTz CMP and Py-Th-TzTz CMP were calculated from CV results.

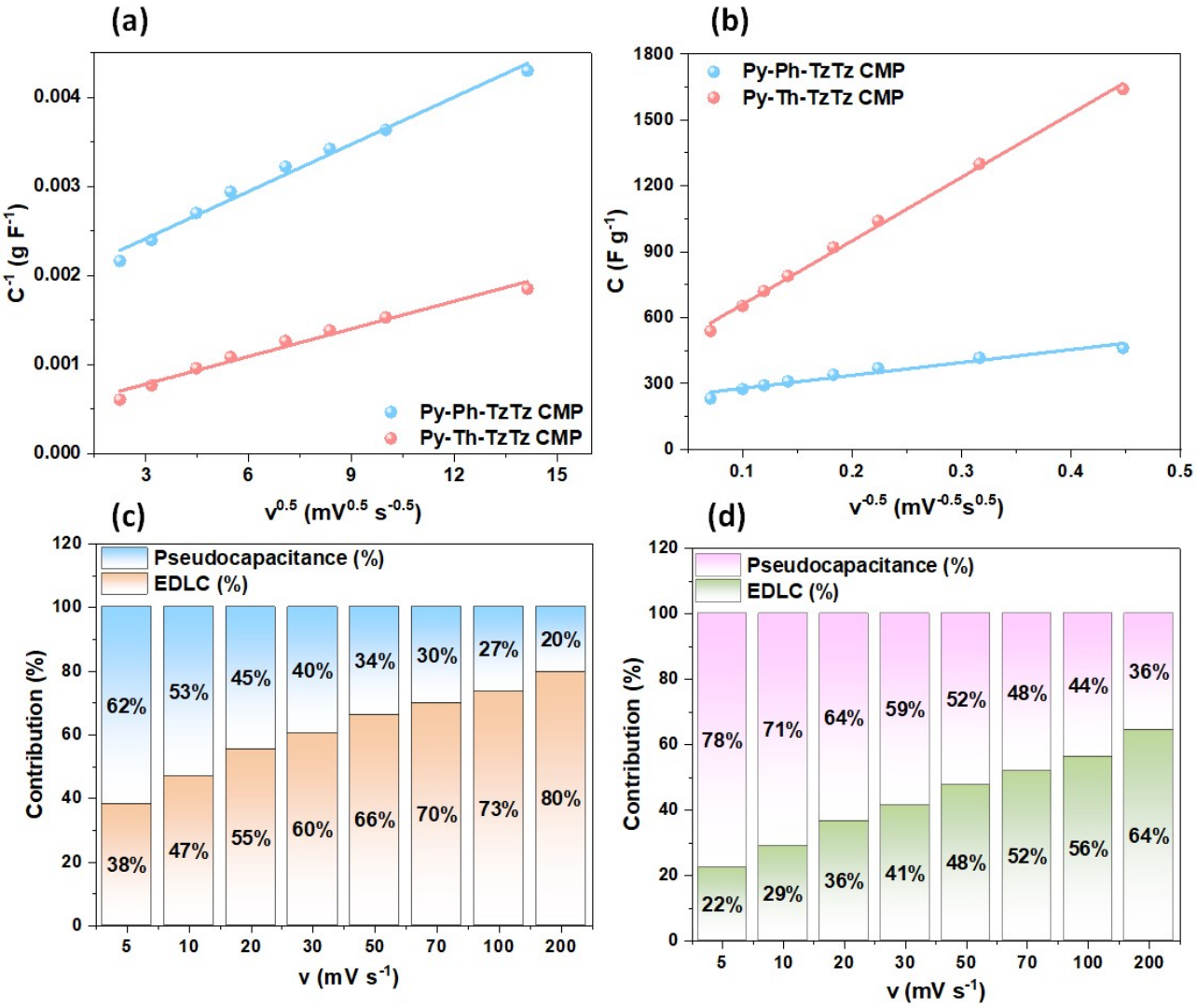

Figure S12. (a) Plots of reciprocal of areal capacitance (C^{-1}) against the square root of scan rate ($v^{0.5}$), (b) plots of gravimetric capacitance against the reciprocal of the square root of scan rate ($v^{-0.5}$), and (c, d) the percentage capacitance contribution of (a, c) Py-Ph-TzTz CMP and (b, d) Py-Th-TzTz CMP.

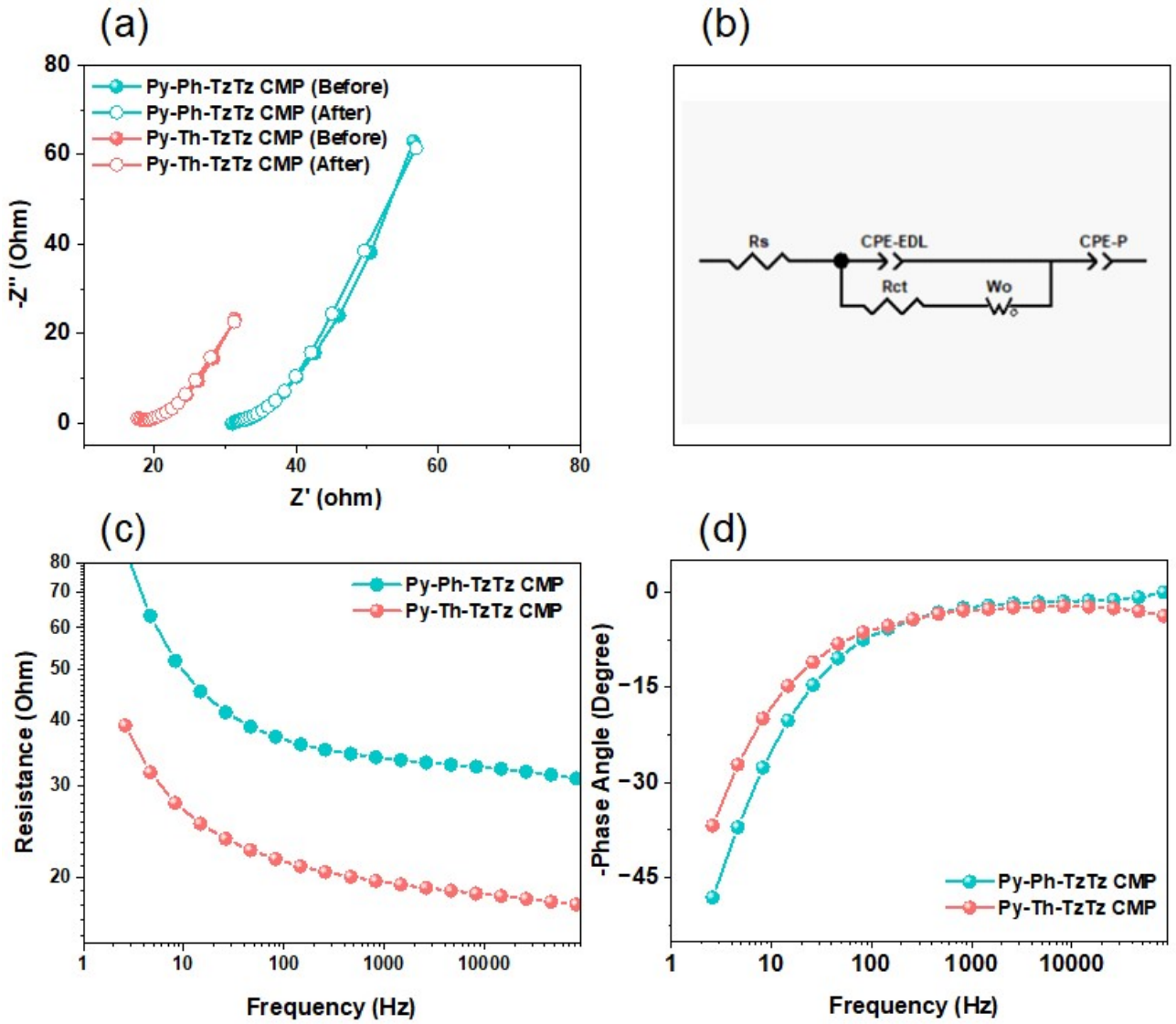

Figure S13. EIS fitting of (a) Nyquist plot of Py-Ph-TzTz and Py-Th-TzTz CMPs, (b) equivalent fitted circuit of the Py-Th-TzTz CMP, (c) Bode plot of frequency-dependant resistance, and (d) Bode plot of frequency-dependant phase angles for the symmetric device of Py-Ph-TzTz CMP and Py-Th-TzTz CMP.

Table S1. TGA data of Py-Ph-4CHO, Py-Th-4CHO, Py-Ph-TzTz CMP, and Py-Th-TzTz CMP.

Sample	$T_{d5\%}$ (°C)	$T_{d10\%}$ (°C)	Char Yield (wt.%)
Py-Ph-4CHO	**320**	**340**	**31**
Py-Th-4CHO	**289**	**384**	**52**
Py-Ph-TzTz CMP	**371**	**502**	**67**
Py-Th-TzTz CMP	**260**	**352**	**63**

Table S2. The atomic weight percentages of carbon (C), nitrogen (N), and sulfur (S) atoms in the Py-Ph-TzTz CMP and Py-Th-TzTz CMP.

Sample	C (%)	N (%)	S (%)
Py-Ph-TzTz CMP	**81.8**	**9.2**	**8.9**
Py-Th-TzTz CMP	**69.3**	**13.1**	**17.5**

Table S3. The XPS fitting data of Py-Ph-TzTz CMP and Py-Th-TzTz CMP.

Sample	C (%)			N (%)		S (%)	
	C-C/C=C (%)	C=N/C=S (%)	C-N/C-S (%)	N-C (%)	N=C (%)	$S2p_{3/2}$ (%)	$S2p_{1/2}$ (%)
Py-Ph-TzTz CMP	**89.8**	**5.4**	**4.7**	**32.7**	**38.8**	**78.1**	**21.9**
Py-Th-TzTz CMP	**48.4**	**49.9**	**1.6**	**43.5**	**34.2**	**89.5**	**10.5**

Table S4. A comparison of the supercapacitor performance between Py-Ph-TzTz CMP and Py-Th-TzTz CMP in three-electrode systems using previously described electrodes

Electrode	Capacitance	Ref.
Py-Ph-TzTz CMP	**464 F g^{-1} at 1 A g^{-1}**	**This work**
Py-Th-TzTz CMP	**625 F g^{-1} at 1 A g^{-1}**	**This work**
Cz-Cz CMP	43.70 F g^{-1} at 0.5 A g^{-1}	S1

Cz-TP CMP	67.38 F g^{-1} at 1 A g^{-1}	S1
Pure AQ	42 F g^{-1} at 1 A g^{-1}	S2
TPE-DDSQ-POIP	22 F g^{-1} at 1 A g^{-1}	S3
Car-DDSQ-POIP	23 F g^{-1} at 1 A g^{-1}	S3
HPC-0	48 F g^{-1} at 1 A g^{-1}	S4
H-THAQ	15 F g^{-1} at 1 A g^{-1}	S5
CoPc-CMP	13.8 F g^{-1} at 1 A g^{-1}	S6
Py-Ph-BDT CMP	429 F g^{-1} at 1 A g^{-1}	S7
Py-DSDA-COP/SWCNTs	171 F g^{-1} at 1 A g^{-1}	S8
Py-Ph-Pery-CMP	300 F g^{-1} at 0.5 A g^{-1}	S9
Try-TPET-BT	157 F g^{-1} at 0.5 A g^{-1}	S10
P-PT-CMP	400 F g^{-1} at 0.5 A g^{-1}	S11
Try-Ph-TPE-CMP	245 F g^{-1} at 0.5 A g^{-1}	S12

Table S5. A comparison of the supercapacitor performance between Py-Ph-TzTz CMP and Py-Th-TzTz CMP using previously described electrodes (based on symmetric SCs coin cells).

Electrode	Capacitance	Ref.
Py-Ph-TzTz CMP	**108 F g^{-1} at 1 A g^{-1}**	**This work**
Py-Th-TzTz CMP	**226 F g^{-1} at 1 A g^{-1}**	**This work**
IITR-COF-1	30.5 F g^{-1} at 0.12 A g^{-1}	S13
PAN/Lignin-800-1//PAN/Lignin-800-1	58.77 F g^{-1} at 0.5 A g^{-1}	S14
PDPT-CNT	126 F g^{-1} at 0.5 A g^{-1}	S15
CoFePBA/P3/CC/AC	161.12 F g^{-1} at 0.5 A g^{-1}	S16
AQ-NPCs//TN-NPCs	86 F g^{-1} at 1 A g^{-1}	S17
PCCGNs-1:4	97.1 F g^{-1} at 0.5 A g^{-1}	S18
PTPA@MWNT-4	216 F g^{-1} at 1 A g^{-1}	S19
NOSHPCs-1:2:2	134.88 F g^{-1} at 0.5 A g^{-1}	S20

References

[S1] S. F. Saber, S. U. Sharma, J. T. Lee, A. F. M. EL-Mahdy and S. W. Kuo. Carbazole-conjugated microporous polymers from Suzuki–Miyaura coupling for supercapacitors. *Polymer* **2022**, *254*, 125070. doi.org/10.1016/j.polymer.2022.125070.

[S2] B. Guo, Y. Yang, Z. Hu, Y. An, Q. Zhang, X. Yang, and Wang, H. Redox-active organic molecules functionalized nitrogen-doped porous carbon derived from metal-organic framework as electrode materials for supercapacitor. *Electrochim. Acta*, **2017**, *223*, 74–84. doi.org/10.1016/j.electacta.2016.12.012.

[S3] M. G. Mohamed, W.C. Chen, A. F. M. EL-Mahdy and S. W. Kuo. Porous organic/inorganic polymers based on double-decker silsesquioxane for high-performance energy storage. *J. Polym. Res*. **2021**, *28*, 219. doi.org/10.1007/s10965-021-02579-x.

[S4] L. Wan, J. Wang, L. Xie, Y. Sun and K. Li. Nitrogen-enriched hierarchically porous carbons prepared from polybenzoxazine for high-performance supercapacitors. *ACS Appl. Mater. Interfaces*, **2014**, *6*, 15583–15596. DOI: 10.1021/am504564q.

[S5] L. Xu, R. Shi, H. Li, C. Han, M. Wu, C. P. Wong, F. Kang, B. Li. Pseudocapacitive anthraquinone modified with reduced graphene oxide for flexible symmetric all-solid-state supercapacitors. *Carbon* **2018**, *127*, 459-68. DOI: 10.1016/j.carbon.2017.11.003.

[S6] L. Mei, X. Cui, Q. Duan, Y. Li, X. Lv, H. G. Wang. Metal Phthalocyanine-Linked Conjugated Microporous Polymer Hybridized with Carbon Nanotubes as a High-Performance Flexible Electrode for Supercapacitors. *Int. J. Hydrogen Energy* **2020**, *45*, 22950-22958. doi.org/10.1016/j.ijhydene.2020.06.208.

[S7] T. A. Gaber, L. R. Ahmed, and A. F. M. El-Mahdy. Efficient faradaic supercapacitor energy storage using redox-active pyrene- and benzodithiophene-4,8-dione-tethered conjugated microporous polymers. *J. Mater. Chem. A*, 2023. **11**,19408-19417.

[S8] M. Ejaz, M. G. Mohamed, W. C. Huang and S. W. Kuo. Pyrene-based covalent organic

polymers with nano carbonaceous composites for efficient supercapacitive energy storage. *J. Mater. Chem. A*, 2023. **11**, 22868-22883.

[S9] P. N. Singh, M. G. Mohamed, S. V. Chaganti, S. U. Sharma, M. Ejaz, J. T. Lee and S. W. Kuo. Rational Design of Ultrastable Conjugated Microporous Polymers Based on Pyrene and Perylene Units as High-Performance Organic Electrode Materials for Supercapacitor Applications. *ACS Appl. Energy Mater*. 2023, **6**, 8277–8287. doi.org/10.1021/acsaem.3c01391.

[S10] T. H. Weng, M. G. Mohamed, S. U. Sharma, I. M. A. Mekhemer, H. H. Chou and S. W. Kuo. Rationally Engineered Ultrastable Three-Dimensional (3D) Conjugated Microporous Polymers Containing Triptycene, Tetraphenylethene, and Benzothiadiazole Units as Exceptional High-Performance Organic Electrodes for Supercapacitors. *ACS Appl. Energy Mater*. 2023, **6**, 9012–9024. doi.org/10.1021/acsaem.3c01933.

[S11] M. G. Mohamed, S. V. Chaganti, S. U. Sharma, M. M. Samy, M. Ejaz, J. T. Lee, K. Zhang and S. W. Kuo. Constructing Conjugated Microporous Polymers Containing the Pyrene-4,5,9,10-Tetraone Unit for Energy Storage. *ACS Appl. Energy Mater*. 2022, **5**, 10130–10140. doi.org/10.1021/acsaem.2c01842.

[S12] T. H. Weng, M. G. Mohamed, S. U. Sharma, S. V. Chaganti, M. M. Samy J. T. Lee and S. W. Kuo, Ultrastable Three-Dimensional Triptycene- and Tetraphenylethene-Conjugated Microporous Polymers for Energy Storage. *ACS Appl. Energy Mater*. 2022, **5**, 14239–14249. doi.org/10.1021/acsaem.2c02809.

[S13] Y. Kumar, I. Ahmad, A. Rawat, R.K. Pandey, P. Mohanty and R. Pandey. Flexible Linker-Based Triazine-Functionalized 2D Covalent Organic Frameworks for Supercapacitor and Gas Sorption Applications. *ACS Appl. Mater. Interfaces* 2024, **16**, 11605-11616. doi.org/10.1021/acsami.4c00126.

[S14] Y. Ma, L. Li, X. Wei, C. Li, Q. Bai, Y. Shen and H. Uyama. Polyacrylonitrile-sodium lignosulfonate-derived nitrogen-doped three-dimensional hierarchical porous carbon for

supercapacitors. *J. Ind. Eng. Chem*. 2024, **134**, 495-503. doi.org/10.1016/j.jiec.2024.01.012.

[S15] C. Bathula, I. Rabani, A. Kadam, H. Opoku, S. A. Patil, N. K. Shreshta, J. H. Hwang, Y. S. Seo, and H. S. Kim. Sonochemically exfoliated polymer-carbon nanotube interface for high performance supercapacitors. *J. Colloid Interface Sci*. 2022, **606**, (2022) 1792-1799. doi.org/10.1016/j.jcis.2021.08.136.

[S16] S. He, A. Muslim, G. Adili, S. Rahmat, T. He and R. Yao, Increased Energy Density with Conjugated Polymer-Based Composite Electrode without Power Density Sacrifice. *ACS Appl. Polym. Mater*. 2024, **6**, 10178–10192. doi.org/10.1021/acsapm.4c01109.

[S17] B. Guo, Y. Yang, Z. Hu, Y. An, Q. Zhang, X. Yang, X. Wang and H. Wu. Redox-active organic molecules functionalized nitrogen-doped porous carbon derived from metal-organic framework as electrode materials for supercapacitor. *Electrochimica Acta* 2017, **223**, 74-84. doi.org/10.1016/j.electacta.2016.12.012.

[S18] J. Jiang, M. Wang, W. Zhao, Y. Cao, R. Shi and Z. Wang. Potassium acetate activation strategy for synthesizing multiple heteroatom-doped porous carbons containing 2D nanosheets from polybenzoxazine for supercapacitor applications. *Eur. Polym. J*. 2024, **208**, 112856. doi.org/10.1016/j.eurpolymj.2024.112856.

[S19] H. Zuo, J. Duan, B. Lyu, W. Lyu, Y. Li, X. Mei, and Y. Liao. Carbon Nanotube Template-Assisted Synthesis of Conjugated Microporous Polytriphenylamine with High Porosity for Efficient Supercapacitive Energy Storage. *Macromol. Rapid Commun*. 2024, **45**, 2300238. DOI: 10.1002/marc.202300238.

[S20] J. Jiang, M. Wang, W. Zhao, H. Liu, Y. Wang, P. Song and Z. Wang. Hierarchical porous carbon materials derived from N, O, S-Containing Bio-Based polybenzoxazine for Supercapacitors. *Eur. Polym. J*. 2023, **191**, 112054. doi.org/10.1016/j.eurpolymj.2023.112054.